第 44 卷 第 10 期/2024 年 5 月/光学学报 亮点文章·特邀研究论文

光学学报

耦合等离激元体系的复频率分析

曾可博，张霜*

香港大学物理系新基石科学实验室，香港 999077

摘要 耦合等离激元体系在光场调控、光学传感、光学成像及光电器件等领域中有着广泛应用。目前，阻碍耦合等离激元进一步实用化发展的关键问题是金属材料具有较大的损耗。结合数值仿真方法，从理论上研究了耦合等离激元的损耗机理，并进一步分析复频率光源激励对耦合等离激元体系的作用，提出了通过合成复频率波的方法来补偿损耗，从而恢复被削弱的耦合共振信号。所提优化手段具有泛用性高且无需额外成本的优势，研究结果对耦合等离激元体系在各个领域中的研究发展具有借鉴意义，有利于挖掘该体系的潜在应用价值。

关键词 物理光学；纳米光学；等离激元；复频率波；光学传感

中图分类号 O436 **文献标志码** A **DOI**：10.3788/AOS240692

1 引 言

在纳米光学领域中，耦合等离激元是一种重要的研究对象。等离激元是指在导体表面与介质交界处，自由电子在光波驱动下集体振荡的现象。这种集体振荡的电子运动形式可以大大压缩光与物质相互作用的尺度，进而在亚波长级别上实现对光的操纵[1]。在此基础上，当两个或更多的等离激元模式存在耦合通道并被同时激发时，它们会相互影响而形成新的等离激元状态，这就是耦合等离激元。等离激元的耦合强度和方式决定了耦合等离激元体系的共振频率、辐射衰减等光学特性。通过改变微纳结构的大小、形状或材料等来改变耦合效应，可以增强光和物质之间的相互作用，从而高效调控光场的强度、相位和偏振等性质。目前，耦合等离激元已被广泛应用于光学传感[2-5]、光学成像[1,6]、光电芯片[7-8]及光伏设备[9]等领域。例如，在光学传感中，通过测量耦合等离激元的共振变化，可以实现对环境中化学或生物物质的高灵敏度检测；在光学成像中，利用耦合等离激元的亚波长传播能量，可以实现突破衍射极限的超分辨成像。然而，金属材料的固有损耗以及共振结构的辐射损耗限制了耦合等离激元的强度、寿命和传播距离，并削弱了耦合共振信号，使其容易被噪声信号淹没，降低了耦合等离激元器件的灵敏度等性能指标，阻碍了其在实际应用中的进一步发展。该问题的一种解决方案是在体系中加入光学增益材料来补偿损耗[10-11]，但会引入噪声和不稳定性[12]，在实践中受到较大限制。另一种方案是采用复频率波（后文简称复频波）作为光源，时间衰减的复频波在理论上已被证明可以减少材料损耗[13-16]。目前复频率光源的制造仍面临巨大的挑战，在实验上还未被实现过。为了避开实验上的困难，最近有一种新的复频波的制造方法被提出，且成功实现了超分辨成像[17]和超高灵敏度的生物分子传感[18]。该方法仅基于普通的实频率实验数据，便可计算合成复频波的实验结果而无需任何额外的成本，且合成复频波有效地恢复了因损耗丢失的光学信息。

对于耦合等离激元体系，合成复频波的方法同样具有补偿其损耗的潜能。本文将以经典的耦合等离激元结构为例，利用基于有限时域差分（FDTD）法的数值仿真软件（CST Studio Suite，后文将此软件简称为CST）开展研究，从理论方面解释耦合等离激元共振信号被削弱的机理，并尝试分析在复频波作用下耦合等离激元体系的光学性质与原始实频率信号进行对比，可以证明合成复频波能够有效增强耦合等离激元的共振信号，为解决其体系损耗、提高器件性能提供了一种切实可行的方法。

2 耦合等离激元周期结构

2.1 不同偏振角度的平面波入射

如图 1(a)所示，考虑由两条在x-y平面上相互垂直的金属棒构成的周期单元，平面波沿z轴向下正入射。金属棒长度$L=190$ nm、宽度$w=30$ nm、厚度$b=20$ nm，两条金属棒的间距$d=20$ nm，周期长度$D=450$ nm；根据该结构的对称性，在偏振角$\theta_u=\pi/4$

收稿日期：2024-03-05；**修回日期**：2024-03-30；**录用日期**：2024-04-07；**网络首发日期**：2024-04-12

项目基金：香港研究资助局研究基金(AoE/P-701/20，17309021)

通信作者：*shuzhang@hku.hk

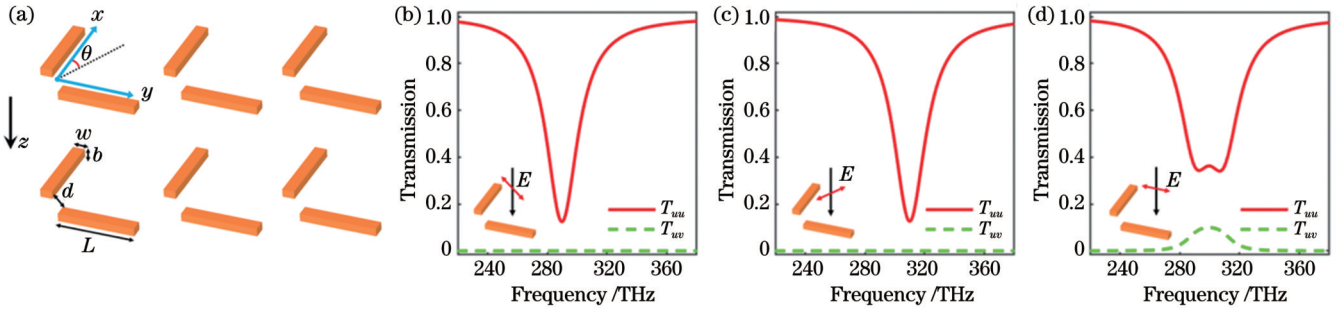

图 1　耦合等离激元周期结构示意图及数值仿真结果。(a)结构参数;(b)偏振角 θ_u 入射光下的同偏振透射谱 T_{uu} 和正交偏振透射谱 T_{uv};(c)偏振角 θ_v 入射光下的同偏振透射谱 T_{vv} 和正交偏振透射谱 T_{vu};(d)偏振角 θ_y 入射光下的同偏振透射谱 T_{yy} 和正交偏振透射谱 T_{yx}

Fig. 1　Schematic diagram and numerical simulation results of coupled plasmonic periodic structure. (a) Structural parameters; (b) transmission spectra of same polarization T_{uu} and orthogonal polarization T_{uv} under incident light with polarization angle θ_u; (c) transmission spectra of same polarization T_{vv} and orthogonal polarization T_{vu} under incident light with polarization angle θ_v; (d) transmission spectra of same polarization T_{yy} and orthogonal polarization T_{yx} under incident light with polarization angle θ_y

(沿结构对角线)和 $\theta_v=3\pi/4$(沿结构反对角线)的条件下,存在两个本征模式 u 和 v,通过 CST 软件数值仿真不同偏振角的平面波入射后结构被激发的响应可以验证这一点。仿真中设定金属棒的材料为银,并采用 Drude 模型计算其介电常数 ε_{Ag}(等离子频率 $\omega_p=1.258\times10^{16}$ rad/s,金属损耗率 $\gamma_p=7.29\times10^{13}$ rad/s)。图 1(b)、(c)是 CST 仿真得到的透射谱线,其中 E 为电场,可以看到在偏振角 θ_u 和 θ_v 的入射下,结构在频率 $\omega=290$ THz 和 $\omega=310$ THz 处有共振信号,且与其正交的偏振态透射率几乎为 0,意味着没有发生偏振转化,则 u 和 v 确实为该耦合等离激元的本征模式。再考虑偏振角 $\theta_x=0$ 或 $\theta_y=\pi/2$ 入射的情况,这两种偏振条件实际上是等价的。此时入射光在 u 和 v 上的投影皆不为 0,由此两个模式都会被激发并相互作用,产生新的耦合共振信号。如图 1(d)所示,在偏振角 θ_y 的入射下,结构在频率 $\omega=300$ THz 处有新的共振信号,且由于模式 u 和 v 在偏振角 θ_x 上也有分量,因此发生了偏振转化,与其正交的偏振态也产生了共振响应。耦合共振信号的强度由两个因素决定,一个是本征模式 u 和 v 之间的耦合强度,它受材料参数和结构的几何参数影响,例如减小两根金属棒的距离 d 可以增强它们表面电磁场的能量传递,进而增强耦合强度;另一个因素是本征模式 u 和 v 各自的损耗率。由图 1(d)可知,耦合共振信号实际上十分微弱,特别是偏振转化后的透射谱 T_{yx},共振频率 300 THz 处的谷几乎被淹没。

2.2　耦合共振信号的损耗机理

为了通过复频率的手段恢复这种极其微弱的耦合共振信号,接下来将先从一个简单的极化模型出发,结合耦合模理论研究该耦合等离激元结构的损耗机理。

先讨论本征模式 u 和 v 的情况,其表面极化率 $\alpha_{u(v)}$ 可以由洛伦兹模型[19-20]描述,具体为

$$\alpha_{u(v)}=\frac{-g_{u(v)}c\gamma_{u(v)}}{\omega^2-\omega_{0u(v)}^2+\mathrm{i}\omega\gamma_{u(v)}},\tag{1}$$

式中:$g_{u(v)}$ 为本征模式和入射光的耦合系数;$\gamma_{u(v)}$ 为模式损耗率;$\omega_{0u(v)}$ 为模式的共振频率;c 为光速。考虑模式有较大的品质因子,即 $\omega_{0u(v)}\gg\gamma_{u(v)}$,则式(1)可以近似简化为线性模型

$$\alpha_{u(v)}=\frac{-g_{u(v)}c\gamma_{u(v)}/\left(2\omega_{0u(v)}\right)}{\omega-\omega_{0u(v)}+\mathrm{i}\gamma_{u(v)}/2}。\tag{2}$$

对于所考虑的这种很薄的金属结构,基于菲涅耳公式,可以推导出在偏振角 $\theta_{u(v)}$ 入射下的透射系数[20]为

$$t_{u(v)}=\frac{1}{1-\mathrm{i}\omega\alpha_{u(v)}/\left(2cD\right)^2},\tag{3}$$

式中:D 为单元的周期长度。为了简便,我们可以定义一个正比于极化率的物理量 $P_{u(v)}$ 并改写透射系数,具体公式为

$$\begin{cases}P_{u(v)}=\dfrac{\alpha_{u(v)}}{\left(2cD\right)^2}=\dfrac{-G_{u(v)}}{\omega-\omega_{0u(v)}+\mathrm{i}\gamma_{u(v)}/2}\\ t_{u(v)}=\dfrac{1}{1-\mathrm{i}\omega P_{u(v)}}=\dfrac{\omega-\omega_{0u(v)}+\mathrm{i}\gamma_{u(v)}/2}{\omega-\omega_{0u(v)}+\mathrm{i}\left(\gamma_{u(v)}/2+G_{u(v)}\omega\right)}\end{cases},\tag{4}$$

式中:比例系数 $G_{u(v)}=g_{u(v)}\gamma_{u(v)}/\left(8\omega_{0u(v)}cD^2\right)$。由式(4)可知,模式的损耗率 $\gamma_{u(v)}$ 决定了 $P_{u(v)}$ 的共振展宽,进而间接影响了透射共振峰的宽度。显然,$\gamma_{u(v)}$ 越大会导致透射峰宽越大而拉平共振信号,降低其品质因子。基于 CST 仿真结果,采用最小二乘法拟合数据可以验证式(4)的准确性并得到各个关键参数值。如图 2 所示,拟合模型得到的透射系数 t_{uu} 和 t_{vv} 的振幅和相位与仿真结果吻合得很好,拟合得到的本征模式 u 和 v 参数:$G_u=2.85\times10^{12}$,$\omega_{0u}=2.896\times10^{14}$ rad/s,$\gamma_u=9.20\times10^{12}$ rad/s;$G_v=2.68\times10^{12}$,$\omega_{0v}=3.098\times10^{14}$ rad/s,$\gamma_v=9.36\times10^{12}$ rad/s。

基于上述模型,可以考虑偏振角 θ_y 下激发的耦合共振信号。根据耦合模理论,本征模式 u 和 v 相互作用

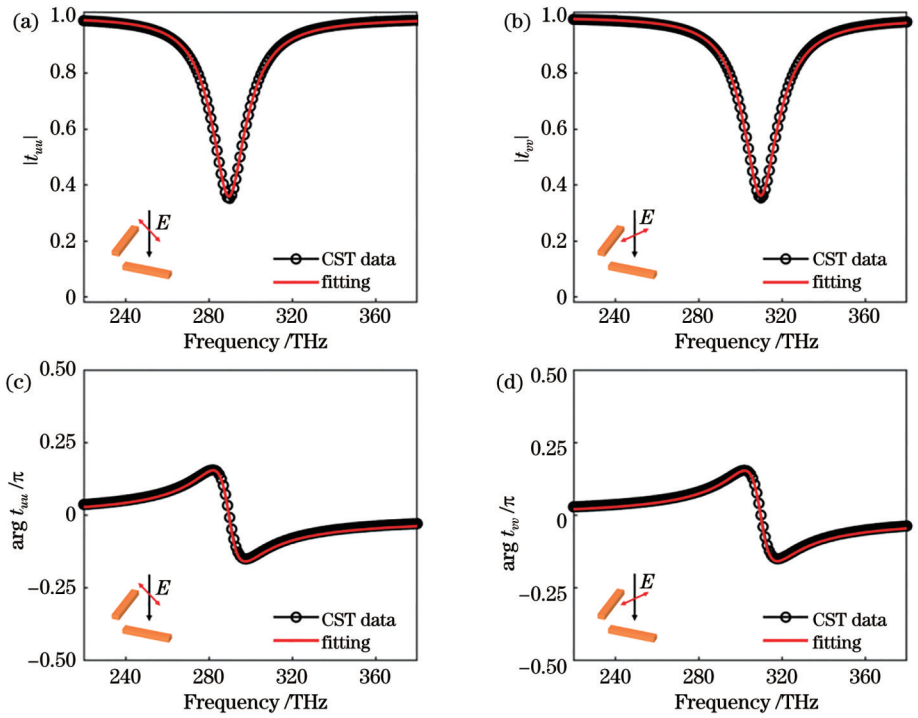

图 2　透射系数的数值仿真和理论拟合结果对比。(a)透射振幅$|t_{uu}|$;(b)透射振幅$|t_{vv}|$;(c)透射相位 arg t_{uu};(d)透射相位振幅 arg t_{vv}

Fig. 2　Comparison of numerical simulation and theoretical fitting results of transmission coefficient. (a) Transmission amplitude $|t_{uu}|$; (b) transmission amplitude $|t_{vv}|$; (c) transmission phase arg t_{uu}; (d) transmission phase arg t_{vv}

的耦合模式可以由特征矩阵[21-23]描述,

$$\begin{pmatrix} \omega_{0u}-\mathrm{i}\gamma_u/2 & \kappa \\ \kappa & \omega_{0v}-\mathrm{i}\gamma_v/2 \end{pmatrix}\begin{pmatrix}\alpha\\ \beta\end{pmatrix}=\omega\begin{pmatrix}\alpha\\ \beta\end{pmatrix}, \tag{5}$$

式中:κ为两个模式的耦合强度因子。求解该特征矩阵便可得到耦合后新的共振模式$\omega_{\pm}$,具体表示为

$$\omega_{\pm}=\frac{\omega_{0u}+\omega_{0v}}{2}-\frac{\mathrm{i}\left(\gamma_u+\gamma_v\right)}{4}\pm\frac{\sqrt{\left[\omega_{0u}-\omega_{0v}-\mathrm{i}\left(\gamma_u-\gamma_v\right)\right]^2+4\kappa^2}}{2}。 \tag{6}$$

由式(5)可知$\gamma_u\approx\gamma_v$,因此式(6)还可以简化为

$$\omega_{\pm}=\frac{\omega_{0u}+\omega_{0v}}{2}-\frac{\mathrm{i}\left(\gamma_u+\gamma_v\right)}{4}\pm\frac{\sqrt{\left(\omega_{0u}-\omega_{0v}\right)^2+4\kappa^2}}{2}。 \tag{7}$$

式(7)描述了耦合共振信号轮廓的形成机理。$\omega_{\pm}$即图 1(d)的透射谱线中的两个共振峰,频率中心为$\left(\omega_{0u}+\omega_{0v}\right)/2$,即原模式的共振频率平均(谱线上的谷)。式(7)中的第二项表明$\omega_{\pm}$的损耗率是原模式u和v的平均;第三项代表$\omega_{\pm}$两个模式的距离,耦合强度因子κ越大,两个模式被劈裂得越远。而谱线上谷的凹陷深度可以用来衡量耦合等离激元的性能,当κ相对较小而模式损耗率又比较大时,便会导致两个靠近的模式$\omega_{\pm}$有较大的共振展宽且高度重叠,使得谱线上的谷被抹平变浅,这正是耦合等离激元共振信号会被损耗削弱的原因。一般而言,耦合因子κ需要通过重新设计微纳结构参数来调制,在实际运用中存在局限性。

3　合成复频波方法

回顾公式(4),假设给实频率ω附加一个虚部变为复频率$\tilde{\omega}=\omega-\mathrm{i}\tau/2$,$\tau$为虚拟增益因子,则有复频波激发下的极化率和透射系数为

$$\begin{cases}\tilde{P}_{u(v)}=\dfrac{-G_{u(v)}}{\omega-\omega_{0u(v)}+\mathrm{i}\left(\gamma_{u(v)}-\tau\right)/2}\\ \tilde{t}_{u(v)}=\dfrac{1}{1-\mathrm{i}\omega P_{u(v)}}=\dfrac{\omega-\omega_{0u(v)}+\mathrm{i}\left(\gamma_{u(v)}-\tau\right)/2}{\omega-\omega_{0u(v)}+\mathrm{i}\left(\gamma_{u(v)}/2-\tau/2+G_{u(v)}\omega\right)}\end{cases}。 \tag{8}$$

此时$\tilde{P}_{u(v)}$的损耗率等价为$\left(\gamma_{u(v)}-\tau\right)$,若$\tau>0$即波源随时间衰减,模式损耗将可以被补偿,从而间接使共振峰宽变窄。需要注意的是,当$\tau=\gamma_{u(v)}$时,$\tilde{P}_{u(v)}$的损耗为0,意味着其共振展宽也趋于0,但$\tilde{t}_{u(v)}$的共振峰展宽并不等于0。这是因为式(8)中分母仍存在$\mathrm{i}G_{u(v)}\omega$这一虚数项,因此继续增大τ使得$\tilde{P}_{u(v)}$由损耗变为增益状态,可以进一步缩窄透射共振峰,提高其品质因子。当然,为了保持物理上的不发散,τ的取值不能无限增大,必须保证$\tilde{t}(\tilde{\omega}_{0u(v)})<1$,由此可给出$\tau$的约束条件:$\tau<\gamma_{u(v)}+G_{u(v)}\omega_{0u(v)}$。

基于上述讨论,时间衰减的复频波确实能补偿本

征模式 u 和 v 的损耗，而由式(7)可知，u 和 v 的损耗率减小同样意味着耦合模式 $\omega_{\pm}$ 的损耗率减小。因此，复频波有能力增强被削弱的耦合共振信号。但由于缺乏真实的复频率光源，在实验中直接通过复频波激发来增强耦合等离激元仍是无法实现的，这里考虑合成复频波的方法来代替真实复频波源。首先，考虑一个时间截断的复频波

$$E_{\mathrm{T}}(t_0)=E_0\exp(-\mathrm{i}\tilde{\omega}t_0)\theta'(t_0), \tag{9}$$

式中：E_0 为初始振幅；$\theta'(\cdot)$ 为截断函数。其中截断函数 $\theta'(t_0)$ 在时间 $t_0\geqslant 0$ 时为 1，在时间 $t_0<0$ 时为 0，这是为了保证复频波的收敛性。接着，对公式(9)作傅里叶变换，得到 $E_{\mathrm{T}}(\omega)=1/\left[\mathrm{i}(\tilde{\omega}-\omega)\right]$，因此可以将式(9)重新写成为

$$E_{\mathrm{T}}(t_0)=\frac{E_0}{2\pi}\int_{-\infty}^{+\infty}\frac{1}{\mathrm{i}(\tilde{\omega}-\omega')}\exp(-\mathrm{i}\omega' t_0)\mathrm{d}\omega'。 \tag{10}$$

式(10)说明复频波可以看作由无穷个实频波与相应系数的乘积叠加而成的结果，且随着实频波的频率越远离中心频率，系数 $1/\left[\mathrm{i}(\tilde{\omega}-\omega')\right]$ 将越趋于 0，这意味着通过有限频域的实频波可以构造出近似的复频波。另一方面，基于式(10)，对于系统的任意线性响应 $F(\omega)$，复频波激发下的响应同样也可以表示为实频率响应的合成，具体表达式为

$$F(\tilde{\omega})=\int_{-\infty}^{+\infty}F(\omega')\frac{1}{\mathrm{i}(\tilde{\omega}-\omega')}\times\exp\left[-\mathrm{i}(\tilde{\omega}-\omega')t_0\right]\mathrm{d}\frac{\omega'}{2\pi}。 \tag{11}$$

因此，只需要得到基于实频率波激发下的透射响应，便可求得耦合等离激元在复频波激发下的透射响应，进而实现利用复频波补偿损耗，增强共振信号的目标。在实际应用中，取足够大的频率范围并对式(11)作离散化处理，过程可表示为

$$t(\tilde{\omega})\approx\sum_n t(\omega_n)\frac{1}{\mathrm{i}(\tilde{\omega}-\omega_n)}\times\exp\left[-\mathrm{i}(\tilde{\omega}-\omega_n)t_0\right]\Delta\omega/2\pi。 \tag{12}$$

式中：$\Delta\omega$ 为频率采样间隔。

复频波下的透射率 $T(\tilde{\omega})=\left|t(\tilde{\omega})\right|^2$。至此，耦合等离激元的复频波下的透射可以由实频率透射的数据计算合成，下面将采用CST仿真得到的实频率数据进行验证。如图 3(a)、(b)所示，基于图 1(d)中的透射谱，计算合成了不同虚拟增益 τ 激发下的透射响应 $T_{yy}(\tilde{\omega})$ 和 $T_{yx}(\tilde{\omega})$。可以看到，随着 τ 的增大，谱线中的谷凹陷越来越深，原来微弱的耦合共振特征被逐渐增强至清晰，这充分说明了合成复频波方法能补偿损耗，恢复被削弱的共振信号。图 3(c)～(f)分别展示了不

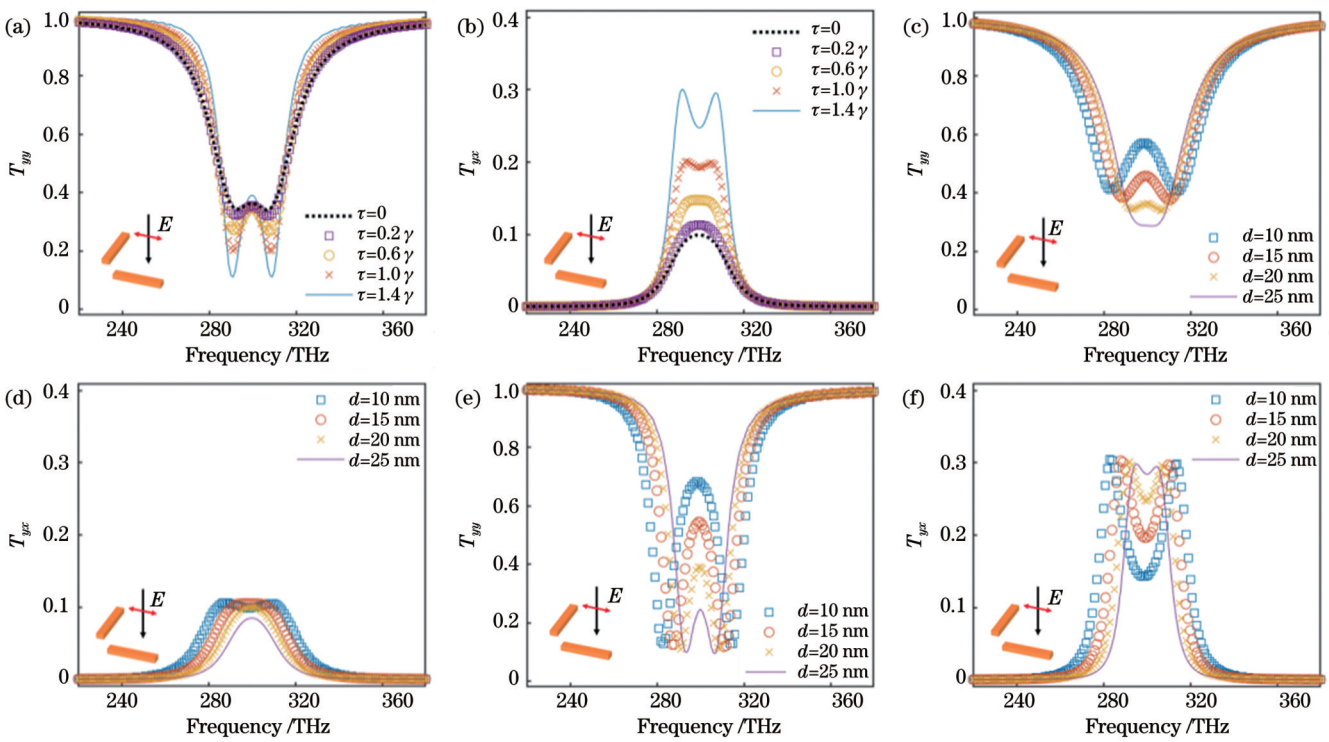

图 3　实频率和复频率激励下的透射谱。(a)(b)不同虚拟增益因子 τ 条件下的透射谱 T_{yy} 和 T_{yx}，$\gamma=\gamma_u$；(c)(d)不同耦合强度(不同间距 d)条件下的实频率激励的透射谱 T_{yy} 和 T_{yx}；(e)(f)不同耦合强度(不同间距 d)条件下的复频率激励的透射谱 T_{yy} 和 T_{yx}，$\tau=1.4\gamma_u$

Fig. 3　Transmission spectra of real frequency and complex frequency excitation. (a)(b) T_{yy} and T_{yx} under different virtual gain factors τ conditions, $\gamma=\gamma_u$; (c)(d) T_{yy} and T_{yx} of real frequency excitation under different coupling intensity (different gap d) conditions; (e)(f) T_{yy} and T_{yx} of complex frequency excitation under different coupling intensity (different gap d) conditions, $\tau=1.4\gamma_u$

同耦合强度(通过调节金属棒间距d)下合成复频波的增强效果。对比图 3(c)、(d)中的实频率原始谱线,图 3(e)、(f)中的复频波透射谱都显著增强,即使原始共振峰几乎重合至谷且难以分辨,合成复频波方法也能将其恢复到劈裂状态。这些结果进一步验证了合成复频波的有效性和泛用性。

4 结 论

对耦合等离激元体系的损耗问题展开研究,基于金属微纳结构的数值仿真,理论上分析了耦合等离激元的共振信号形成机理以及受限因素,表明了在耦合强度较小的情况下,较大的等离激元损耗将严重削弱其耦合共振信号的强度。紧接着,分析了复频率波源激励对耦合等离激元体系的影响,表明了具有时间衰减的复频波能补偿体系的模式损耗,并采用了由实频率波响应合成复频波响应的方法,计算获得了耦合等离激元的复频波透射谱。结果表明,合成复频波方法能很好地实现通过复频率激励来补偿损耗的效果,从而增强被削弱的耦合共振信号。研究结果为解决耦合等离激元体系的损耗问题提供了一种切实可行且泛用的方法,有助于推动该体系在光学成像、光谱技术、光学传感等领域中的进一步发展。

参 考 文 献

[1] Schuller J A, Barnard E S, Cai W S, et al. Plasmonics for extreme light concentration and manipulation[J]. Nature Materials, 2010, 9(3): 193-204.

[2] Mejia-Salazar J R, Oliveira O N, Jr. Plasmonic biosensing[J]. Chemical Reviews, 2018, 118(20): 10617-10625.

[3] Brolo A G. Plasmonics for future biosensors[J]. Nature Photonics, 2012, 6: 709-713.

[4] Taylor A B, Zijlstra P. Single-molecule plasmon sensing: current status and future prospects[J]. ACS Sensors, 2017, 2(8): 1103-1122.

[5] Chung T, Lee S Y, Song E Y, et al. Plasmonic nanostructures for nano-scale bio-sensing[J]. Sensors, 2011, 11(11): 10907-10929.

[6] Barnes W L, Dereux A, Ebbesen T W. Surface plasmon subwavelength optics[J]. Nature, 2003, 424(6950): 824-830.

[7] Zia R, Schuller J A, Chandran A, et al. Plasmonics: the next chip-scale technology[J]. Materials Today, 2006, 9(7/8): 20-27.

[8] Luk'yanchuk B, Zheludev N I, Maier S A, et al. The Fano resonance in plasmonic nanostructures and metamaterials[J]. Nature Materials, 2010, 9(9): 707-715.

[9] Atwater H A, Polman A. Plasmonics for improved photovoltaic devices[J]. Nature Materials, 2010, 9(3): 205-213.

[10] Fang A, Koschny T, Wegener M, et al. Self-consistent calculation of metamaterials with gain[J]. Physical Review B, 2009, 79(24): 241104.

[11] Grgić J, Ott J R, Wang F W, et al. Fundamental limitations to gain enhancement in periodic media and waveguides[J]. Physical Review Letters, 2012, 108(18): 183903.

[12] Stockman M I. Spaser action, loss compensation, and stability in plasmonic systems with gain[J]. Physical Review Letters, 2011, 106(15): 156802.

[13] Baranov D G, Krasnok A, Alù A. Coherent virtual absorption based on complex zero excitation for ideal light capturing[J]. Optica, 2017, 4(12): 1457-1461.

[14] Kim S, Lepeshov S, Krasnok A, et al. Beyond bounds on light scattering with complex frequency excitations[J]. Physical Review Letters, 2022, 129(20): 203601.

[15] Li H N, Mekawy A, Krasnok A, et al. Virtual parity-time symmetry[J]. Physical Review Letters, 2020, 124(19): 193901.

[16] Tetikol H S, Aksun M I. Enhancement of resolution and propagation length by sources with temporal decay in plasmonic devices[J]. Plasmonics, 2020, 15(6): 2137-2146.

[17] Guan F X, Guo X D, Zeng K B, et al. Overcoming losses in superlenses with synthetic waves of complex frequency[J]. Science, 2023, 381(6659): 766-771.

[18] Zeng K B, Wu C C, Guo X D, et al. Synthesized complex-frequency excitation for ultrasensitive molecular sensing[J]. eLight, 2024, 4(1): 1.

[19] Zheng G X, Mühlenbernd H, Kenney M, et al. Metasurface holograms reaching 80% efficiency[J]. Nature Nanotechnology, 2015, 10(4): 308-312.

[20] Ye W M, Guo Q H, Xiang Y J, et al. Phenomenological modeling of geometric metasurfaces[J]. Optics Express, 2016, 24(7): 7120-7132.

[21] Zeng P, Cadusch J, Chakraborty D, et al. Photoinduced electron transfer in the strong coupling regime: waveguide-plasmon polaritons[J]. Nano Letters, 2016, 16(4): 2651-2656.

[22] Törmä P, Barnes W L. Strong coupling between surface plasmon polaritons and emitters: a review[J]. Reports on Progress in Physics, 2015, 78(1): 013901.

[23] Yang J H, Sun Q, Ueno K, et al. Manipulation of the dephasing time by strong coupling between localized and propagating surface plasmon modes[J]. Nature Communications, 2018, 9: 4858.

Complex Frequency Analysis of Coupled Plasmonic Systems

Zeng Kebo, Zhang Shuang*

New Cornerstone Science Laboratory, Department of Physics, University of Hong Kong, Hong Kong 999077, *China*

Abstract

Objective Due to the strong light-matter interactions, coupled plasmonic systems have broad applications in such areas as light manipulation, optical sensing, optical imaging, and optoelectronic devices. However, the inherent dissipation of

materials and radiation dissipation of resonant structures limit the strength, service life, and propagation distance of coupled plasmonics, weakening the coupling signals and reducing the sensitivity and other performance of coupled plasmon devices. One possible solution is to add optical gain materials into the systems to compensate for the dissipation, but the utilization of gain materials is still limited because of the introduction of noise and instability. Another possibility is to employ complex frequency waves as light sources. It has been theoretically demonstrated that complex frequency waves with temporal attenuation can restore information losses. Unfortunately, producing complex frequency waves in real optical systems still faces significant challenges and has not been yielded experimentally. Currently, a novel method for synthesizing complex frequency waves has been proposed to be successfully applied to super-resolution imaging and highly sensitive biosensing. Therefore, we adopt this method to compensate for the dissipation of coupled plasmonic systems, thereby enhancing their resonance signals and avoiding experimental challenges. We hope that our study can benefit the development of coupled plasmonic systems for various potential applications.

Methods We employ a periodic plasmonic structure composed of two perpendicular silver rods as an example to investigate the mechanism behind the attenuation of coupled resonance in coupled plasmonic systems. The structure is simulated by the finite-difference time-domain (FDTD) method using CST Studio Suite software. In the simulation, a plane wave with different polarization angles (45°, 90°, and 135°) is normally incident onto the structure with the periodic boundary to obtain the transmission coefficients, with the permittivity of silver described by the Drude model. Furthermore, we combine the Lorentz polarization model with temporal coupled-mode theory to analyze the interaction of plasmonic modes.

Results and Discussions The simulation results (Fig. 1) show that under an incident wave whose polarization angle equals 45° (135°), the eigenmode of the plasmonic structure appears at 290 THz (310 THz) with no conversion of orthogonal polarization. Subsequently, a wave with 90° polarization can simultaneously excite the two eigenmodes and generate the coupled signal of the structure. Theoretical analysis shows that the strength of the coupled plasmonic signals depends on the frequency difference and the dissipation of the eigenmodes. Under the relatively small frequency difference and large dissipation, the two coupled new modes will have a large broadening and high overlap in the spectra, causing the coupled valley in the center to be weakened and shallowed. The Lorentz polarization model shows that complex frequency waves with temporal attenuation can enhance the weakened signals by reducing the dissipation of the eigenmodes. Based on Fourier transform analysis, the linear responses excited by complex frequency waves can be synthesized by the coherent combination of multiple real frequency responses. The calculation results (Fig. 3) show that synthesized complex frequency waves with different virtual gains can gradually enhance the coupled signals, where the coupled valley in the spectral line becomes increasingly deeper. Additionally, the synthesized complex frequency wave method is also effective for different coupling strengths (distance adjustment between silver rods). Even if the original signal is difficult to distinguish, this method can also restore it to the split state.

Conclusions We study the dissipation in coupled plasmonic systems based on numerical simulations using CST Studio Suite software and theoretical analysis that incorporates the Lorentz polarization model and temporal coupled modes theory. Meanwhile, we explain the formation mechanism of coupled plasmonic signals and identify their limiting factors. Our findings suggest that under small coupling strength, larger dissipation of plasmonic systems will significantly hamper their coupled resonance. Then, we analyze the influence of complex frequency wave excitation on coupled plasmonic systems, and the results indicate that complex frequency waves with temporal attenuation can compensate for the dissipation of the system and restore the weak signal. To avoid the experimental difficulties of complex frequency waves in real optical systems, we employ a new method for synthesizing complex frequency responses via real frequency waves to calculate the transmission spectrum of the coupled plasmonic structure excited by complex frequency waves. Our results demonstrate that the proposed method can compensate for the dissipation of the coupled plasmonic structure in different conditions, significantly enhancing the coupled signals with almost no additional cost. The findings provide a practical and general method for solving the long-standing dissipation of coupled plasmonic systems, facilitating further applications of coupled plasmonic systems such as optical imaging, spectroscopy technology, and optical sensing.

Key words physical optics; nano optics; plasmonic; complex frequency wave; optical sensing